Metabolic switch in the aging astrocyte evidenced via integrative approach comprising network and transcriptome analyses

Alejandro Acevedo[3], Felipe Torres[4,5,8], Miguel Kiwi[4,5], Felipe Baeza-Lehnert[6], L. Felipe Barros[6], Dasfne Lee-Liu[1,2]*, Christian González-Billault[1,2,7]*

Affiliation:

1. Laboratory of Cellular and Neuronal Dynamics, Faculty of Sciences, Universidad de Chile.
2. Geroscience Center for Brain Health and Metabolism (GERO), Santiago.
3. Instituto de Nutrición y Tecnología de Alimentos (INTA), Universidad de Chile.
4. Department of Physics, Universidad de Chile.
5. Center for the Development of Nanoscience and Nanotechnology, CEDENNA.
6. Centro de Estudios Científicos (CECs), Valdivia.
7. The Buck Institute for Research on Aging, Novato, USA.
8. Department of Physics, Center for Advanced Nanoscience, University of California, USA.

***Correspondence:**

Christian González-Billault, chrgonza@uchile.cl or Dasfne Lee-Liu, dnlee@uc.cl

ABSTRACT

Central energy metabolism is a pivotal process dysregulated during brain aging. The neuron and the astrocyte form an extensive interconnected metabolic network that allows achieving the high energy demand required by the neuron to propagate information in the brain. While most of this energy is utilized to re-establish cation gradients in neurons and glial cells, which specific genes in the neuron-astrocyte metabolic network are essential for continuous neurotransmission and are responsible for cognitive decline during brain aging remains largely unknown.

To identify these gene products, we used a novel approach to analyze the neuron-astrocyte metabolic network, integrating network flux (optimality) and structure (centrality) and determined how the contribution of each gene in the network affected its function. Genes with the highest optimality and centrality scores were termed "hub genes." They were searched in astrocyte and neuron transcriptomic databases to identify "differential hub genes," which were differentially expressed during neurotransmission or aging.

The identified differential hub genes suggest that during brain aging: 1) The neuron suffers energetic deficit by substantial downregulation of Krebs cycle genes including *mdh1* and *mdh2* (malate-aspartate shuttle), while the astrocyte undergoes a metabolic switch from aerobic glycolysis to oxidative phosphorylation, hampering the supply of lactate to the neuron; 2) Branched-chain amino acid (BCAA) degradation hub genes were downregulated, including hub gene *dld*, an integrative gene that encodes for a subunit in BCAA-, pyruvate- and α-ketoglutarate dehydrogenase complexes; and 3) Increased ketone body synthesis in the neuron and augmented astrocytic utilization, in line with neuronal energy deficit in favor of astrocytes.

Differential hub gene identification was robust and resulted in novel candidates for future pre-clinical studies targeting energy metabolism to prevent age-associated cognitive decline. Importantly, our approach narrows down the number of candidate genes identified in

transcriptomic databases by two orders of magnitude. This method may be applied to other metabolic cellular models in future omics studies.

KEYWORDS

Astrocyte, neuron, metabolism, aging, transcriptome, neurotransmission, neurodegeneration

INTRODUCTION

Energy metabolism, essential for brain function, is one of the main processes dysregulated during brain aging (reviewed in (Mattson & Arumugam 2018; Pellerin & Magistretti 1994)). Although the brain constitutes only 2% of total body mass, it represents 20-25% of total body energy expenditure (Attwell & Laughlin 2001; Bonvento & Bolaños 2021), where most of it is used for re-establishing cation gradients after neurotransmission (Harris *et al.* 2012), a process mediated by sodium/potassium-ATPase pumps (Baeza-Lehnert *et al.* 2018; Erecinska & Silver 1994). To meet this high energy demand, the neuron and astrocyte form a two-cell metabolic network *(the neuron-astrocyte metabolic network)* with extensive metabolite exchange (Bonvento & Bolaños 2021; Bélanger *et al.* 2011). One example of metabolic exchange is the astrocyte-neuron lactate shuttle (ANLS) (Pellerin & Magistretti 1994). The astrocyte performs aerobic glycolysis, converts pyruvate into lactate, and then transports it to the neuron to fuel ATP synthesis via oxidative phosphorylation (Mächler *et al.* 2016; Zuend *et al.* 2020). The neuron-astrocyte metabolic network also performs the glutamate-glutamine cycle (GGC). In the GGC, astrocytes take up glutamate -the main excitatory neurotransmitter in the central nervous system- after neurotransmission. Inside the astrocyte, glutamate is converted into glutamine, shuttled back to the neuron, and re-converted into glutamate for a new neurotransmission cycle (Magistretti & Allaman 2015; Hasel *et al.* 2017; Schousboe 2019; Hyder *et al.* 2006). The ANLS, GGC, and the exchange of sodium and potassium constitute essential metabolic interactions between neurons and astrocytes, and they are closely related to energy metabolism. Indeed, energy availability is vital to ensure proper neurotransmission. However, during human brain aging, metabolism becomes dysregulated in the brain. Healthy aged human individuals display slower mitochondrial metabolism and glutamate-glutamine cycle neuronal flux (-28%) when compared with healthy young individuals. In comparison, astroglial mitochondrial flux is 30% faster (Boumezbeur *et al.* 2010). In rats, adult primary astrocyte cultures also display a higher mitochondrial oxidative metabolism when compared with astrocytes derived from young rats (Jiang & Cadenas 2014). To date, the only intervention demonstrated to extend lifespan in several model organisms is caloric restriction, a metabolic

intervention where animal models are fed a diet consisting of 60-70% of the calorie intake in a regular diet (Mattison *et al.* 2017). This further supports the role of energy metabolism during aging. Metabolic challenges like the ketogenic diet (Newman *et al.* 2017; Roberts *et al.* 2017) and intermittent fasting that aim to mimic the metabolic state entered during caloric restriction have also been shown to extend lifespan and health-span (Dias *et al.* 2021). Furthermore, a phase II clinical trial using a fasting-mimicking diet improved metabolic health (Wei *et al.* 2017).

The complexity of brain aging is determined by the diversity and number of metabolic pathways that contribute to energy balance. The molecular mechanisms underlying age-associated dysregulation of brain energy metabolism remain mostly unknown. Complex systems - particularly metabolic pathways- are studied by modeling them as networks, which allows to simulate and probe complex phenomena, such as aging, in a computationally tractable and interpretable fashion (O'Brien *et al.* 2015; Zweig 2016). Here, we present a novel network-wise mapping complex interactions into a graph representation approach to discover energy-related genes in the neuron-astrocyte metabolic network that may contribute to brain aging. We used a genome-scale model of the neuron-astrocyte metabolic network (Lewis *et al.* 2010) and analyzed it using complementary flux and network-based methods. Flux-based methods allowed us to identify reactions critical for maintaining optimal neurotransmission.

On the other hand, network-based methods (centrality) searched for reactions that may modulate neurotransmission via network-wide effects. This analysis provided us with a set of genes (metabolic hub genes) that are key for neurotransmission in terms of flux distribution and network structure. Next, we determined which metabolic hub genes showed differential abundance associated with neurotransmission and/or brain aging in the neuron and/or astrocyte, thus getting a final set of genes called *differential hub genes*. These gene set represents a validation of network analysis contrasting numerical predictions with experimental data, including expected and novel results.

Functional annotation analysis of differential hub genes led to the following main findings: 1) Gene expression changes in both the neuron and astrocyte suggest an energetic deficit in the neuron, mainly by substantial downregulation of tricarboxylic acid (TCA) cycle in the aging neuron; 2) In line with the neuronal energy deficit, our results suggest that the aging astrocyte undertakes a metabolic switch from aerobic glycolysis to oxidative metabolism, where glucose is directed to CO_2 instead of lactate; 3) Impaired branched-chain amino acid degradation in both the neuron and astrocyte, mainly supported by downregulation of the *dld* gene during aging. This gene encodes for a subunit of the branched-chain amino acid (BCAA) dehydrogenase complex, which catalyzes an early step in BCAA degradation; 4) Altered ketone body metabolism, where gene expression changes in the neuron agree with an increased synthesis during brain aging, while in the aging astrocyte *bdh1* is upregulated. This gene catalyzes the interconversion between acetoacetate and β-hydroxybutyrate, the main two ketone bodies required for ketone body utilization. These findings further support that energy metabolism is favored in the astrocyte, in detriment of neuronal energy supply; 5) Downregulation of genes associated with synaptic transmission in the neuron, including downregulation of Na/K-ATPase pumps in the aging neuron, and lower glutamate synthesis in both neuron and astrocyte; 6) Our results suggest that the aging neuron downregulates genes that supply the one carbon and tetrahydrofolate (THF) pool, which is required for the synthesis of the methylation precursor S-adenosylmethionine (SAM) and antioxidant glutathione synthesis. Instead, the aging astrocyte displays expression changes that agree with an increase in the THF pool available for glutathione synthesis as an antioxidant strategy, which is also in line with the metabolic switch into an oxidative metabolism in the astrocyte (which requires more antioxidation).

The genes identified here are valuable candidates for future studies to understand the molecular mechanisms of healthy brain aging and prevent brain age-associated failure using energy metabolism as a target. We also highlight how our approach significantly provides a robust and tractable number of final gene candidates for future studies, using an integrative analysis of the two-cell neuron-astrocyte metabolic network, which may be applied to other metabolic models.

RESULTS

Workflow overview. Our approach considered a genome-scale constraint-based model that tackles three aspects of the metabolic network conformed by neurons and astrocytes: (i) short-lived and fast response to the neurotransmission-derived workload, (ii) invariant neuronal concentrations of cytosolic ATP and ADP, (iii) and long-term impairment upon aging. The former aspect was addressed by coupling four key events triggered by neurotransmission: neuronal ATP consumption derived from sodium efflux, ATP supply via oxidative phosphorylation in neurons, the ANLS, and the GGC. These four events were flux-coupled by combining them into a pseudo-reaction, denoted as the *metabolic objective.* Next, the flux passing through the metabolic objective was maximized to account for the fast response. The second aspect (constant energy availability) constrained this maximization, meaning that we imposed a *steady-state*. This procedure yielded the *optimal metabolic response,* which corresponds to the metabolic fluxes that give rise to the maximal rate for the metabolic objective without undermining energy availability and comprising the whole genome-scale network. Next, we identified (throughout the entire network) reactions that can perturb the previously-calculated optimal metabolic response and denoted it as the *sensitivity set*. This group of reactions represented a sort of "interface" through which the optimal metabolic response can be perturbed or impaired. Consistently with the nature of neurotransmission, this "interface" (or sensitivity set) communicates short-lived and fast perturbations under steady-state. Up to this point, our model encoded the transitory and brief nature of neurotransmission. In order to incorporate long-term non-stationary effects, like the ones spread during aging, we took into account the structural (topological) context of the interface (sensitivity set). Network topology encodes wide-spectrum phenomena beyond steady-state and non-limited to short-lived events. In this sense, a deeper regulation layer was determined using topology-based analysis. This second layer comprises nodes that, via topology-wise effects, promote/inhibit the interactions in the sensitivity set. Since this last layer was identified by employing *centrality-based analysis,* we denoted it as the *centrality set.* Taken together, we propose that mechanisms giving rise to aging-derived energetic dysregulation take place in both the sensitivity and centrality set. We

designated the union of the sensitivity and centrality sets as metabolic *hub genes*. We followed this analysis using gene expression transcriptome databases to determine which metabolic hub genes displayed differential abundance associated with neurotransmission and/or brain aging in the neuron and/or astrocyte. The databases utilized contained separate gene expression data for the neuron and astrocyte during neurotransmission (Hasel *et al.* 2017) and aging (Consortium 2020). The intersection between the hub genes set and genes differentially expressed in neurotransmission and/or aging was defined as *differential hub genes*.

Flux balance analysis identifies critical hub genes for glutamatergic neurotransmission function

We identified reactions (and transports) able to perturb the optimal functioning of neurotransmission. To such an aim, we employed a constraint-based model of the neuron-astrocyte metabolic network, calculated its optimal flux-state, and carried out a sensitivity analysis (for details, see methods and supplementary material sections 1.1 to 1.4). The optimal state represents the flux distribution that optimizes our metabolic objective. This objective was the maximization of the flux rates of the astrocyte-neuron lactate shuttle (ANLS), glutamate-glutamine cycle (GGC), and sodium removal by the Na/K-ATPase pump (Figure 1a-c). This maximization simulates the metabolic state when glutamatergic neurotransmission takes place (the complete rationale behind this assumption is exposed in the supplementary sections 1.2 - 1.4)

We formulated our FBA's constraints from previously published flux values (Baeza-Lehnert *et al.* 2018; Fernández-Moncada *et al.* 2018). Regarding these fluxes, Baeza-Lehnert et al. (Baeza-Lehnert *et al.* 2018) showed that under stimulation, neurons extrude sodium ions at a rate of 350 µM/s. Accordingly, we fitted the astrocytic glucose consumption to match the reported neuronal sodium efflux (350 µM/s) while keeping the other constraints constant (for details about the other constraints, see Supplementary Section 1.7). As shown in Figure 1d, we reached precisely 350 µM/s in the solution of the FBA. Physiologically, astrocytic and neuronal metabolisms highly depend on glucose and oxygen availability. Hence, we checked if our FBA

solution was sensitive to changes in oxygen and glucose. To this end, we computed the Phenotypic Phase Planes (PhPPs) subjected to glucose and oxygen uptake rates (for details regarding PhPPs, refer to supplementary section 2). In PhPP analysis, when planes containing the optimal solution have a non-zero slope, the optimal state depends on oxygen and carbon sources (for details regarding PhPPs, refer to Supplementary Section 1.6). Figures 1d-g show the neuron-astrocyte metabolic network optimal solution (red-filled circle) in a glucose and oxygen consumption range, *i.e.*, the PhPP. Here, contour level variation (represented by the color map) in the PhPPs indicates that our phenotype depends on glucose and oxygen. This result validates our model in terms of sensitivity. Also, our optimal state was associated with complete (aerobic) glucose oxidation, *i.e.*, six oxygen molecules oxidized one glucose molecule (Figure S1a). In comparison, the ATP yield was close to 29 ATP molecules per glucose molecule (Figure S1b). In addition, Figures 1e and f show that the ANLS and the GGC were active at the optimal state. Lastly, from Figure 1g, we can safely assume that the optimal solution is unique since it locates on a vertex. Our model was mathematically consistent and agreed with the biological phenotype of neurons and astrocytes undergoing neurotransmission.

In addition to the optimal fluxes, we computed the sensitivity of the optimal solution concerning each flux. Sensitivity indicates the extent to which a specific increase in flux perturbs the FBA solution. We determined how optimality variables, *i.e., sensitivity* and flux values, were distributed throughout the neuron-astrocyte metabolic network, shown in Figure 1h. Here, we observed that nodes from the same cell were highly connected with each other. This distribution gave rise to a two-core structure surrounded by sparsely connected nodes. We found that depending on the optimality variable (flux or sensitivity), nodes having high values allocated preferentially in one of the cells. This phenomenon is shown in Figure 1i for flux and Figure 1j for sensitivity. More precisely, nodes with high flux were prevalent in the neuron (Figure 1i), while nodes with high sensitivity were primarily allocated in the astrocyte (Figure 1j).

Next, we integrated flux and sensitivity into a single value. To this end, we constructed a two-element optimality vector consisting of the flux and the sensitivity for each reaction. Then, we used the length (L1 norm) of this optimality vector as our optimality index and named it *absolute optimality*, a value that condenses information from both flux and sensitivity.

We used the absolute optimality values to define crucial nodes to achieve optimal flux distribution during neurotransmission, *i.e.*, *optimality hubs*. In this sense, all nodes larger than the absolute optimality threshold were considered optimality hubs. We used an unsupervised clustering method to determine our threshold (see Methods). Both in the neuron and astrocyte, the threshold coincided with the 90th percentile of the data (Figure 1k). Figure 1l shows fluxes and sensitivities of the optimality hubs separated by cell type. We observed that most reactions with non-zero flux did not coincide with those with non-zero sensitivity. This pattern emerged because flux sensitivity informs about the potential a reaction has in controlling the value of the optimal solution. In this line of thought, a reaction that already has flux has deployed its potential, leaving little or no space for improvement (zero sensitivity). Besides, zero flux reactions (with non-zero sensitivity) may improve the objective value if (certain) constraints were relaxed. Also, it could be observed that the majority of non-zero flux nodes were neuronal, while non-zero sensitivity nodes were astrocytic (Figure 1l).

Figure 1m shows the enrichment pathway analysis of optimality hubs using KEGG MODULE, a collection of manually defined functional units. Enriched pathways related to astrocytic optimality hubs comprised GABA and glycogen biosynthesis, while neuron-represented pathways were mainly associated with the tricarboxylic acid (TCA) cycle and ketone bodies (Figure 1m). In addition, Figure 1n shows the enrichment analysis of optimality hubs based on the REACTOME pathway database. Here, glycogen and nucleotide metabolism pathways were predominant in the astrocyte, while the TCA cycle and ketone body metabolism prevailed in neurons (Figure 1n).

Up to this point, we have characterized the neuron-astrocyte metabolic network by focusing on neurotransmission and the underlying flux optimization that ensures its proper functioning. Reaction flux provided the metabolic phenotype deployed in terms of metabolite conversion or transport, while reaction sensitivity indicated a reaction's potential in modulating the objective function. Therefore, the identified hub genes represent nodes crucial for glutamatergic neurotransmission function in terms of flux.

Contribution of each node or reaction by analyzing intrinsic network structure

To find genes that control the sensitive subsystem using network topology, we used *centrality metrics* (Borgatti 2006). Centrality measures how well integrated a node is into the entire network. Hence centrality informs about the non-local influence that a given node has over the rest of the nodes (details in Supplementary Section 2.3). This concept of nodal influence can be extended to a group of nodes; in this case, we can describe the level of influence a group has over the rest of the network; this is often referred to as group centrality. In our case, we identified nodes (reactions) that can modulate the centrality of the sensitivity subsystem (group centrality). A reaction-node-based network represents the quintessence of the astrocyte-neuron interaction, capturing the essential contribution of long-ranged interactions between these cells. The contribution of each reaction was evaluated in the neuron-astrocyte metabolic network to the centrality of the sensitivity subsystem by determining the fold change of the ratio between basal (unperturbed) subsystem centrality and the centrality of the same subsystem when the node in question is removed (perturbed). This fold change represents a *nodal contribution* to the centrality of the sensitive subsystem. Importantly, each node in the neuron-astrocyte metabolic network was associated with four types of nodal contributions, each one corresponding to a certain kind of centrality metric that was calculated for the sensitive subsystem. Briefly, we employed two metrics of centrality that measure the distance of the subsystem to the rest of the nodes in the neuron-astrocyte metabolic network, and the other two metrics that count the paths in which the sensitive subsystem participates. Figure 2a shows the nodal contributions of each cell. Here, on average, astrocytic contributions were

more significant than the contributions of the neuron. We also studied how nodal contributions correlates with each other. Pairwise correlations were estimated by considering the four nodal contributions per node as samples, while each node was regarded as a variable. Figure 2b shows the unsupervised hierarchical clustering of the correlation matrix between nodes. Here, the two-cell structure of the neuron-astrocyte metabolic network roughly emerged. This level of separation between nodes of different cells indicates that correlations between nodes from the same cell tend to be mostly positive.

On the other hand, correlation between nodes from different cells showed a greater extent of negative correlation (Figure 2b). We performed a dimensionality reduction over nodal contribution keeping nodes as samples to confirm that the correlation matrix represents the two-cell structure. Principal Component Analysis (PCA) also confirmed the emergence of the two-cell structure from the correlations, *i.e.*, nodes from the same cell type showed a tendency to cluster together (Figure 2c). In order to have a single quantity for topological relevance, we computed the length (L1 norm) of each vector containing the contributions per node. We named such a nodal index as *absolute centrality*. These values are shown on the right-hand side of the heatmap (Figure 2b). We selected nodes using the same criteria as in the previous section on optimality (Figure 2d). The reactions associated with those nodes are shown in Figure 2e. Here, the absolute centrality is separated by cell, and consistent with the distributions of nodal contributions (Figure 2a), the astrocyte had the highest values for absolute centrality. Next, we extracted the genes associated with the centrality hubs, thus defining a set called *central hub genes.* We conducted the same pathway enrichment analyses used for optimal hub genes. Figures 2f and g show that enriched pathways in neurons and astrocytes were mainly related to vitamins, such as pantothenate (Vitamin B) and cofactors needed for the biosynthesis of Coenzyme A and fatty acid and amino acid metabolism.

Differential hub genes during neurotransmission and aging

Thus far, we have generated an "optimality hub gene set" and a "centrality hub gene set." We obtained the union between both sets, which yielded a complete list which we denoted *hub genes*. The next step was to determine which hub genes have been reported as differentially abundant in response to glutamatergic neurotransmission and/or during brain aging. For this, we used the databases described below. Differential abundance values (fold-change (neurostimulation/basal) or age-coefficient (aged/young) as reported by the authors were considered.

For neurotransmission, we used a database that reported transcriptomic changes occurring in neurons and astrocytes, which were grown in a mixed culture setting and then sequenced using RNA-seq as a single sample. Reads belonging to neurons and astrocytes were separated using bioinformatics, which was possible because primary neurons were obtained from rat embryos, while astrocytes from early postnatal mice (Hasel *et al.* 2017). The authors reported 4441 genes with differential abundance, in response to neurostimulation, in the neuron and 1307 in the astrocyte during neurotransmission (FC ≥1.3 or ≤0.77 and padj-SSS-value < 0.05). As mentioned before, this dataset comes from cells grown in a mixed culture and therefore were in contact with each other before and after neurostimulation, yielding robust transcriptional changes that span the neuron-astrocyte metabolic network.

For brain aging, we used the single-cell RNA-seq database generated by the Tabula Muris Consortium (Consortium 2020), which reported an age-coefficient (equivalent to the fold-change in non-single cell transcriptomics) for neurons and astrocytes derived from the same mouse brain. This study reported 5415 differentially abundant genes in neurons and 1294 in astrocytes during mouse brain aging when comparing 1-3 months old with 18-30 months old mice (age coefficient threshold at 0.005 reported by authors as equivalent to a 10%-fold change and an FDR threshold of 0.01).

Using this data, we obtained 196 mouse orthologs for hub genes in the neuron (all hub genes were reported originally using human identifiers) and 184 hub genes in the astrocyte. The

intersection between genes reported as differentially abundant in the two transcriptomic databases, and the hub gene set defined previously denoted the "differential hub gene" set.

In response to neurotransmission, we found 53 differential hub genes in the neuron and 14 differential hub genes in the astrocyte. We identified 73 differential hub genes in the neuron during aging and 26 differential hub genes in the astrocyte.

Differential hub genes in the neuron suggest a metabolic deficit and impaired synaptic transmission during brain aging

We performed a KEGG pathway enrichment analysis followed by manual curation (see Methods) to obtain a functional characterization of differential hub genes in neurotransmission and brain aging. Figure 3 shows KEGG pathways enriched in neuronal differential hub genes during neurotransmission (Fig. 3a) and brain aging (Fig. 3b), with node colors indicating whether they were up (red nodes) or downregulated (blue nodes) during each process.

We identified five main biological processes with relevant changes when comparing neurotransmission and brain aging through manual curation. The first group was associated with central energy metabolism associated with KEGG pathways "Pyruvate metabolism", "Citrate cycle (TCA cycle)" and "Central carbon metabolism in cancer" (Fig. 3, blue). We decided to include the latter, given that metabolic changes observed in cancer, such as the Warburg effect, also occur in the brain. During neurotransmission, we observed upregulation of *acss1*, a mitochondrial enzyme that synthesizes acetyl-CoA from acetate, and of *pdha1*, which codes for a subunit of the pyruvate dehydrogenase complex (PDC) (Fig. 3a, blue). Upregulation of both enzymes agrees with increased acetyl-CoA levels, which enters the TCA cycle, suggesting high levels of oxidative phosphorylation. Instead, during aging, we observed downregulation of all genes, except for one, involved in the same three KEGG pathways mentioned above. Notably, most reactions belong to the TCA cycle, and *pdha1*, *pdhb,* and *dld* encode for the PDC subunits,

strongly suggesting the acetyl-CoA entry into the neuronal TCA cycle and TCA cycle activity are compromised by brain aging.

The second group was associated with synaptic activity, including a cluster of Na/K-ATPase pumps (Fig. 3, orange) and enzymes that catalyze glutamate synthesis (Fig. 3, green). During neurotransmission, they were upregulated, while in brain aging, they were mostly downregulated. Na/K-ATPase pumps are required to re-establish ion gradients after neurotransmission to allow the following cycle of synaptic activity. At the same time, glutamate is the primary excitatory neurotransmitter, for which these results agree with synaptic activity dysregulation during brain aging, with *got1/2* as differential hub genes regulating glutamate levels.

The third group corresponds to the KEGG pathway "Synthesis and degradation of ketone bodies" (Fig. 3, yellow). During neurotransmission, *hmgcs1*, encoding for the cytosolic form of 3-hydroxy-3-methylglutaryl-CoA synthase 1 was upregulated while *hmgcll1* (3-hydroxymethyl-3-methylglutaryl-CoA lyase like 1) was downregulated. *Hmgcs1* catalyzes the formation of HMG-CoA, which is further converted into mevalonate for cholesterol synthesis (as opposed to the mitochondrial isoform *hmgcs2*, which catalyzes the first irreversible step in ketogenesis using the same substrates as hmgcs1). On the other hand, hmgcll1 catalyzes the second irreversible step in ketogenesis and is downregulated. *Oxct1* catalyzes the interconversion between acetoacetyl-CoA and acetoacetate and was found upregulated. These results suggest the downregulation of ketone body synthesis during neurotransmission while favoring an increased degradation or utilization. As opposed to these results, during brain aging in the neuron, it is *hmgcs2* which is upregulated (ketone body synthesis mitochondrial isoform), while *hmgcs1* is downregulated.

Moreover, *oxct1* and *bdh1* are also downregulated. *Bdh1* catalyzes the interconversion between acetoacetate and beta-hydroxybutyrate, the two main ketone bodies. Therefore, the downregulation of *oxct1* and *bdh1* suggests a decrease in ketone body turnover in aged brains.

The fourth group was associated with the KEGG pathway "Valine, leucine, and isoleucine degradation", and therefore refers to branched-chain amino acid (BCAA) degradation (Fig. 3, purple). While enzymes associated with BCAA degradation were downregulated during both neurotransmission and brain aging in the neuron, *dld*, which encodes for a subunit of the BCAA decarboxylase, catalyzing one of the first steps of the degradation of all three BCAA was only downregulated during brain aging, further supporting downregulation of BCAA degradation during aging.

Finally, the fifth group was associated with regulating one-carbon pool levels (Fig. 3, pink), including KEGG pathways "Glycine, serine and threonine metabolism" and "One carbon pool by folate." During neurotransmission, glycine degradation enzymes *alas1* and *amt* were downregulated, while *shmt2*, which feeds the one-carbon pool by producing 5,10-methylenetetrahydrofolate was upregulated. Also, 2/3 enzymes involved in the metabolism of one-carbon pool intermediates were upregulated (Fig. 3a, pink). However, all enzymes (except for one) associated with these two KEGG pathways were downregulated during aging, suggesting a decrease in the one-carbon pool. We present a summary of all these changes in Table 1.

Differential hub gene abundance changes in the astrocyte suggest a metabolic switch during brain aging

Next, we performed an equivalent analysis of KEGG pathway enrichment of differential hub genes in the astrocyte during neurotransmission and brain aging, followed by manual curation. We found lower number of differential hub genes in the astrocyte when compared with the neuron, which led to a lower number of enriched KEGG pathways. Biological processes identified altered in the neuron were also changed in the astrocyte during brain aging.

The first group, associated with central metabolism (Fig. 4, blue), included enriched KEGG pathways "Pyruvate metabolism" during neurotransmission and aging. In contrast, "Central metabolism in cancer" was only enriched during neurotransmission, and "Citrate cycle (TCA cycle)" was only enriched during brain aging. First, we identified differential hub gene *slc2a1*, the leading glucose uptake transporter in the blood-brain barrier (GLUT1), as upregulated during neurotransmission. Furthermore, we observed a switch between the upregulation of *ldha* during neurotransmission (Fig. 4a, blue) to *ldhb* during brain aging (Fig. 4b, blue). These two genes encode for subunits of lactate dehydrogenase, which catalyzes the interconversion between pyruvate and lactate, with *ldha* subunits favoring lactate synthesis and *ldhb* subunits favoring pyruvate. Finally, *pcx* and *acss1* were downregulated during neurotransmission, both encoding for enzymes that feed substrates into the TCA cycle (TCA cycle anabolism). These results agree with a high glucose uptake during neurotransmission by the astrocyte, elevated lactate synthesis, and low TCA cycle flux, suggesting an active astrocyte-neuron lactate shuttle (ANLS). Instead, during aging, *ldhb* favors pyruvate levels and upregulation of *mdh1* and *mdh2*, enzymes involved in the malate-aspartate shuttle which transports NADH into mitochondria, fueling the electron transport chain and favoring ATP synthesis by oxidative phosphorylation (instead of only aerobic glycolysis) in the astrocyte, in detriment of ANLS flux.

The second group was related to branched-chain amino acid (BCAA) degradation (Fig. 4, purple), where *slc7a5*, involved in leucine degradation, was upregulated during

neurotransmission (Fig. 4a, purple). In contrast, *dld*, *aldh6a1,* and *hibadh*, all BCAA degradation genes, were downregulated during brain aging (Fig. 4b, purple). These results strongly suggest BCAA accumulation in the astrocyte during brain aging.

The third group was associated with ketone body degradation/utilization (Fig. 4b, yellow), where *bdh1* was upregulated during brain aging. As mentioned previously, this gene encodes for the enzyme that catalyzes interconversion of acetoacetate and β-hydroxybutyrate, thus suggesting that the aged astrocyte favors ketone body degradation or utilization.

The fourth group was associated with glutamate levels (Fig. 4b, green), including the *abat*, which encodes for an enzyme that degrades GABA converting it into glutamate. *Abat* was found downregulated during astrocyte aging. These results support a metabolic switch in the astrocyte during brain aging that decreases ANLS flux, which is required for meeting the high-energy neuronal demand, promoting ATP synthesis for the astrocyte's use. Furthermore, changes in differential hub genes observed in the neuron also support an energetic deficit in neuronal metabolism.

The fifth group was related to one-carbon pool regulation, where *gcat* was upregulated during aging, while *gldc* was downregulated. *Gcat* activity feeds the one-carbon pool while *gldc* consumes one carbon intermediates. These results strongly suggest that the aging astrocyte favors the one-carbon pool.

Taken together, differential hub gene regulation during brain aging in both cell types suggests that energy expenditure is reallocated towards the astrocyte in detriment of neuronal function, possibly explaining the functional deficit observed during brain aging. A summary of all changes observed in the astrocyte is included in Table 2.

DISCUSSION

The goal of the present work was to identify hub genes, which we defined as those that, when modified or removed, significantly alter glutamatergic neurotransmission in the neuron-astrocyte network. The ultimate aim was to determine which of these hub genes also changed their expression during neurotransmission, allowing us to compare them with hub genes differentially expressed during brain aging in the neuron and/or astrocyte. We denominated this gene group as *differential hub genes*, which have a high probability of playing a pivotal role in neurotransmission, brain function. If they become dysregulated during aging, they represent excellent candidates to explain age-associated cognitive decline.

We performed three consecutive analyses of the neuron-astrocyte metabolic network to identify these genes. The first was flux balance analysis. We defined the metabolic objective of glutamatergic neurotransmission (comprised of the astrocyte-neuron lactate shuttle, ANLS; the glutamate-glutamine cycle, GGC; and the sodium/potassium-ATPase activity pumps). This allowed us to identify optimal hub genes and the sensitive subsystem (formed by several metabolic pathways) that had the highest probability of improving network function when modified. This subset of genes was denominated *optimal hub genes*.

The second analysis was based on network centrality. We used different metrics to determine which nodes in the network, when modified, most affected the sensitive subsystem identified in the first step mentioned above. We denominated the gene subset associated with these nodes as *central hub genes*.

The third analysis used the union of the optimal hub genes and central hub genes sets (resulting in the *hub genes* set) to find which of these had been reported to display differential abundance in response to neurotransmission (Hasel *et al.* 2017), or during brain aging (Consortium 2020), in the neuron and/or astrocyte. The intersection between the hub genes set and genes displaying differential abundance during neurotransmission and/or aging was

denominated *differential hub genes*. For this refined gene subset, we performed KEGG pathway analysis enrichment. We followed this analysis with manual curation to identify the primary biological processes and pathways essential for neuron-astrocyte metabolic network function and which changes could explain age-associated brain functional decline. We found that manual curation was required, given that certain enzymes were associated with KEGG pathways, and a manual search of references did not indicate direct evidence. Also, enzyme isoforms in the KEGG database were assigned to the same reactions without indicating subcellular compartmentalization, which is critical in determining their function.

We divided differential hub genes into the following six categories: 1) Energetic deficit in the neuron; 2) Metabolic switch in the astrocyte from aerobic glycolysis to oxidative metabolism; 3) Impaired branched-chain amino acid degradation; 4) Altered ketone body metabolism; 5) Downregulation of genes associated with synaptic transmission in the aging neuron; 6) Altered one-carbon pool for tetrahydrofolate (THF) synthesis.

Energetic deficit in the aging neuron

Brain energy metabolism has been described as a hallmark of brain aging (Mattson & Arumugam 2018; Cunnane *et al.* 2020), and metabolic deficit in the neuron, particularly during human brain aging, has been reported. Boumezbeur and colleagues (Boumezbeur *et al.* 2010) reported that flux through the tricarboxylic acid (TCA) cycle decreased by 28% in the presynaptic neuron using *in vivo* magnetic resonance spectroscopy. However, the genes involved in this deficit remain largely unknown. Our analyses showed that the most remarkable changes observed in the aging neuron, which agree with an energetic deficit, was the downregulation of TCA cycle genes, including:

1) Subunits of the pyruvate dehydrogenase complex, *dld* (EC:1.8.1.4), *pdha1* (EC:1.2.4.1), *pdhb* (EC:1.2.4.1), and *dlat* (EC:2.3.1.12), which catalyzes the conversion of pyruvate into acetyl-CoA for entry into the TCA cycle and is therefore required for ATP synthesis. Notably, the *dld* gene (EC:1.8.1.4) encodes for a catalytic subunit of three essential dehydrogenase complexes: the

pyruvate dehydrogenase complex, the α-ketoglutarate dehydrogenase complex (α-KGDH), which catalyzes the conversion from α-KG into succinyl-CoA (reaction that produces NADH in the mitochondrial matrix), and the branched-chain amino acid (BCAA) dehydrogenase complex. Its downregulation during neuronal aging severely affects metabolic function (Odievre *et al.* 2005; Brautigam *et al.* 2006). In fact, the hereditary metabolic disease dihydrolipoamide dehydrogenase deficiency (OMIM: 246900) is caused by *loss of function* of *dld*.

2) Downregulation of *mdh1* and *mdh2* in the aging neuron (which encode for isoforms of the malate dehydrogenase enzymes 1 and 2), involved in the malate-aspartate shuttle, which allows shuttling of NADH into the mitochondrial matrix (Minarik *et al.* 2002). This NADH provides electrons for the electron transport chain (ETC). Furthermore, it has been shown that malate-aspartate shuttle enzyme expression decreases with normal aging and can be reverted using dietary restriction (Goyary & Sharma 2008). Furthermore, *loss-of-function* mutations in the *mdh2* gene are associated with severe neurological deficits in children (Ait-El-Mkadem *et al.* 2017).

3) Downregulation of *idh1* and *idh2* (encoding for the enzymes isocitrate dehydrogenases 1 and 2), which catalyze the synthesis of α-ketoglutarate, a metabolite that is central for metabolism and also connects energy metabolism with neurotransmission as it can enter and exit the TCA cycle by being converted into glutamate, the main excitatory neurotransmitter (refer to Fig. 3a and Table 1 for the complete list and description).

These changes are in line with previous findings of metabolic deficit in the neuron during aging and provide both previously reported genes (validating our modeling method) and novel gene targets. An energetic shortage in a cell with such high energy demand is critical and will necessarily lead to dysfunction.

Astrocyte metabolic switch from aerobic glycolysis to oxidative phosphorylation

In line with the energetic deficit in the neuron, given the astrocyte-neuron lactate shuttle, where the astrocyte plays a primary role in fueling the neuron with lactate, differential gene expression in the astrocyte supported a metabolic switch from aerobic glycolysis to oxidative metabolism. This phenotype has been described previously as a "selfish" phenotype adopted by the astrocyte during aging (Jiang & Cadenas 2014), where pyruvate is used for the astrocyte's own ATP synthesis instead of shuttling to the neuron. The lactate dehydrogenase isoenzymes are formed by four subunits of the polypeptides encoded by genes *ldha* and *ldhb*. LDH-5, the isoenzyme formed by 4 *ldha* subunits, favors lactate production, while LDH-1, formed by 4 subunits of *ldhb,* favors pyruvate production (Bittar *et al.* 1996). We found that the *ldha1* gene was upregulated in the astrocyte during neurotransmission, while the *ldhb* upregulated during brain aging, supporting the glycolytic-to-oxidative metabolic switch in the astrocyte. Interestingly, LDH-1 isoenzymes are localized in both neurons and astrocytes. In contrast, LDH-5 isoenzymes are localized exclusively in astrocytes (Bittar *et al.* 1996), making it even more noteworthy that *ldhb* is upregulated in astrocyte aging.

Ldh upregulation occurs during *Drosophila melanogaster* aging, where *loss-of-function* in either neurons or astrocytes leads to an increase in lifespan, while *gain-of-function* reduces lifespan (Long *et al.* 2020). *Ldh* overexpression also leads to increased neurodegeneration and motor function decline, while ldh downregulation is neuroprotective (Long *et al.* 2020). However, specific studies on the *ldha-to-ldhb* switch in astrocytes have not been performed and would be of great interest to understand the mechanisms of functional brain decline during aging.

Furthermore, malate-aspartate shuttle enzymes *mdh1* and *mdh2* were upregulated during astrocyte aging, supporting the oxidative metabolism switch in the astrocyte (Minarik *et al.* 2002). Therefore, our results show that the neuron displays an intrinsic energetic deficit as demonstrated by its expression changes. Additionally, the astrocyte metabolic switch contributes significantly to this energetic neuronal deficit during brain aging.

Impaired branched-chain amino acid degradation

Valine, leucine, and isoleucine are the three branched-chain amino acids (BCAA). Impairment in their degradation is detrimental to overall metabolic health (Solon-Biet *et al.* 2019; Richardson *et al.* 2021; Yu *et al.* 2021). We observed the downregulation of genes involved in BCAA degradation during neurotransmission and aging in the neuron. During neurotransmission, *aldh6a1*, involved in valine degradation (Fig. 3a and Table 1), and *mccc2* involved in leucine degradation, while during aging, *mccc1* (also leucine degradation), *hibadh* (valine degradation), and *dld*, which catalyzes an early step in the degradation of all three BCAA. Importantly, a recent report showed that detrimental effects of BCAA are mediated mainly through isoleucine, and to a lesser extent, by valine (Yu *et al.* 2021). Therefore, it is valid to conclude that *dld* is the relevant differential hub gene causing BCAA degradation impairment and the consequent detrimental effects in the aging neuron.

Significantly, *dld* was also downregulated in the astrocyte. In fact, slc7a5 involved in leucine degradation was upregulated during neurotransmission in the astrocyte, while *dld*, *aldh6a1,* and *hibadh* were downregulated in the aging astrocyte. As mentioned above, *dld* is also a subunit of the pyruvate and α-ketoglutarate dehydrogenase complexes. Its downregulation in both neuron and astrocyte aging supports its importance as a differential hub gene.

Altered ketone body metabolism

Ketone bodies are produced during caloric restriction, the only intervention known to extend lifespan across various organisms (Mattison *et al.* 2017), and several metabolic challenges are being developed to emulate the effects of caloric restriction, including the ketogenic diet (Newman *et al.* 2017; Roberts *et al.* 2017) and intermittent fasting (Dias *et al.* 2021). Our results suggest that differential hub genes are regulated in the neuron such that during neurotransmission, we found a downregulation of ketogenesis, as shown by upregulation of

hmgcs1, which is the cytosolic isoform of *hmgcs2*. This enzyme catalyzes the first rate-limiting step in ketogenesis (Hegardt 1999). However, this enzyme catalyzes cholesterol biosynthesis in the cytosol instead of ketone body synthesis.

Instead, *hmgcs2* was found upregulated during neuronal aging, and *hmgcs1* downregulated, suggesting an upregulation of ketone body synthesis (Hegardt 1999). *Bdh1* (EC:1.1.1.30) and *oxct1* (EC:2.8.3.5) involved in utilizing ketone bodies were downregulated, suggesting downregulation of ketone body degradation during neuronal aging.

In the astrocyte, *bdh1* (EC:1.1.1.30) was upregulated. This gene encodes for the enzyme that catalyzes the interconversion between β-hydroxybutyrate and acetoacetate, the two main ketone bodies, a reaction required for acetoacetate conversion into acetyl-CoA for eventual ATP synthesis (Cunnane *et al.* 2020). Therefore, this suggests an upregulation of ketone body degradation and utilization in the astrocyte during aging.

Our results suggest that ketone body utilization increased during astrocyte aging while the aging neuron upregulated ketogenesis. These results agree with those mentioned above regarding astrocyte energy expenditure being favored over the neuronal demand during brain aging.

Downregulation of genes associated with synaptic transmission in the aging neuron

During synaptic transmission, we observed that the neuron upregulated genes encoding for four sodium/potassium-ATPase (Na/K-ATPase) pumps (Fig. 3a, orange), while four out of five Na/K-ATPase pumps were downregulated during neuronal aging (Fig. 3b, orange). These pumps are required to re-establish neuronal ion gradients after neurotransmission (Erecinska & Silver 1994; Baeza-Lehnert *et al.* 2018). A downregulation of their expression during aging could contribute to neuronal dysfunction. Furthermore, *got1* (EC:2.6.1.1), which synthesizes glutamate from TCA intermediate □-ketoglutarate, is upregulated during neurotransmission,

while *got1* and *got2* (EC:2.6.1.1) were downregulated during brain aging. Since glutamate is the main excitatory neurotransmitter (Reiner & Levitz 2018) and α-ketoglutarate a key metabolic intermediate in the TCA cycle, these two enzymes, in particular, *got1* (the cytoplasmic isozyme), with opposite regulation during neurotransmission and aging, provide a link between central energy metabolism and synaptic activity. Remarkably, activity for the enzyme encoded by *got* is increased in the brain of Alzheimer's disease individuals compared with healthy controls (D'Aniello *et al.* 2005). However, further characterization of the enzyme during pathological or healthy brain aging is still lacking, making it an exciting target for future studies.

Regarding glutamate levels, the enzyme *abat* (EC:2.6.1.19), which also catalyzes the conversion of α-ketoglutarate into glutamate, is downregulated during astrocyte aging. The reaction catalyzed by this enzyme involves the degradation of γ-aminobutyric acid, or GABA, the main inhibitory neurotransmitter.

Taken together, glutamate levels synthesized by differential hub genes *got1, got2,* and *abat* appear to be decreased during both neuron and astrocyte aging. This has a possible detrimental effect on neurotransmission (given a decrease in available glutamate neurotransmitter levels) and, coupled with downregulation of the expression of Na/K-ATPase pumps in the aging neuron, provides valuable future horizons for the molecular mechanisms of brain aging.

Altered one-carbon pool for tetrahydrofolate (THF) synthesis

The final group we observed was defined by KEGG pathways "One carbon pool by folate" (KEGG map00670) and "Glycine, serine and threonine metabolism" (KEGG map00260). These pathways are of interest during brain aging because THF is the precursor for S-adenosylmethionine, the substrate required for methylation, including DNA and histone methylation (Jones *et al.* 2015; Sen *et al.* 2016; McCauley & Dang 2014). This links central energy metabolism with epigenetic modifications: methylation levels decrease during aging (Levine *et al.* 2020; Wang *et al.* 2020; Benayoun *et al.* 2015; Zampieri *et al.* 2015) and is one of

the epigenetic clocks, which can be modified by metabolic challenges such as caloric restriction (Gensous *et al.* 2019). Furthermore, glycine and serine degradation also feed the one-carbon pool (Amelio *et al.* 2014).

We observed the following differences when comparing the neuron during neurotransmission and aging. *Alas1* was downregulated during aging, and the enzyme it encodes for is involved in the glycine cleavage system but produces intermediates that do not feed the one carbon pool (Amelio *et al.* 2014). Therefore, its downregulation increases the availability of glycine for cleavage by *shmt2* (EC:2.1.2.1), which is upregulated during neurotransmission and produces 5,10-Methylene-THF (KEGG map00260).

Furthermore, one carbon pool by folate enzymes *mthfd1l* (EC: 6.3.4.3) and *mthfd2* (EC: 3.5.4.9) were both upregulated during neurotransmission, and they also feed the THF pool (KEGG map00670). Although *mthfd1* (EC: 6.3.4.3) was downregulated during aging (another enzyme that feeds the THF pool), there upregulation of mthfd1l and mthfd2 suggest the predominant result was an increase in the THF pool.

Notably, all enzymes associated with feeding the one carbon/THF pool were downregulated during aging, except for *alas2*. Therefore, the one-carbon and THF pool, used for methionine synthesis, which leads to glutathione synthesis and also SAM (required for methylation), increased during neurotransmission (Voet & Voet 2004), while being downregulated during neuronal aging.

In the astrocyte, we observed differential expression of two enzymes, suggesting that the astrocyte increases the one carbon and THF pool during aging. The first was *gcat* (EC:2.3.1.29), upregulated during aging, which increases glycine levels from threonine degradation (therefore feeds one carbon and THF pool). The second was *gldc* (EC:1.4.4.2), which catalyzes glycine degradation, but the reaction *consumes* THF. This enzyme was downregulated.

CONCLUDING REMARKS

The work reported here employed two network-based approaches combined with bioinformatics transcriptomics analyses. All numerical predictions were cross validated using reported experimental data. The strategy we developed will be of use for identifying hub genes pivotal for the function of other cellular systems. Our findings suggest that the astrocyte undergoes a metabolic switch from aerobic glycolysis to oxidative metabolism, with a concomitant upregulation of THF precursor synthesis required for glutathione synthesis to control the increased oxidative stress caused by this metabolic switch. Additionally, differential hub genes in the neuron show massive metabolic impairment and downregulation of genes required for synaptic transmission. The genes and pathways identified here include genes previously associated with brain aging and novel targets for aging prevention.

METHODS

Neuron-astrocyte metabolic network. Genome-scale metabolic reconstruction (Fang *et al.* 2020; Thiele & Palsson 2010). The model of the metabolic interactions between cell types in the human brain (Lewis *et al.* 2010). Our topological analysis is based on a constraint-based stoichiometric model for the neuron-astrocyte metabolic network. The binary form of the stoichiometric matrix can be interpreted as the incidence matrix of a bipartite network. In our case, such a bipartite network is composed of reactions and metabolites. Since we are interested in finding relevant genes, we used the reaction projection of the bipartite network. This projection was binary and with zero in its diagonal, meaning that it can be viewed as the adjacency matrix for the reactions. We calculated the centrality of each node in the neuron-astrocyte metabolic network and named these values as the baseline centralities. Then, by using the geometric mean, we aggregated the unperturbed centralities by their corresponding metabolic subsystem. We considered two subsystems, namely the energy metabolism of the astrocyte and the neuron. Such aggregated centrality was denoted as the unperturbed subsystem centrality. Then we proceed to remove each node and recompute the aggregated centralities, thus we obtain a given value of the subsystem centralities by every node removal. Each of these subsystem centralities was called perturbed subsystem centrality. The contribution of a node to a given subsystem centrality was computed as the fold change of the quotient between the unperturbed subsystem centrality divided by the perturbed subsystem centrality, which yields the effect of the presence of a given node against its absence.

Centrality measures. We employed connectedness- and Closeness-based measures of centrality to compute the nodal contributions to the centrality of the sensitive group. Connectedness-based measures of centrality were pagerank (Page *et al.* 1999) and Katz centrality (Katz 1953), while Closeness-based measures were closeness (Freeman 1978) and information centrality (Stephenson & Zelen 1989). Mathematical formulations for each centrality metric are presented in Supplementary Sections 2.3.1 and 2.3.2.

Nodal contribution to the centrality of the energy metabolism. Our calculation of nodal contribution is a variation of the formula of the delta centrality (Latora & Marchiori 2007). In our case, a given measure of centrality is calculated for a metabolic subsystem. This subnetwork centrality was defined as the geometric mean between the centralities of the nodes belonging to the metabolic subsystem. The categorization of nodes into metabolic subsystems was extracted from the Virtual Metabolic Human Database (Noronha *et al.* 2019). The subsystem centrality computed for the unmodified network was denoted as unperturbed centrality. Then the node of interest is removed, and the subsystem centrality is recalculated. The nodal contribution is finally estimated as the fold change of the ratio between the perturbed and unperturbed subnetwork centrality.

Pairwise correlations between nodal contributions, hierarchical clustering, and Principal Component Analysis (PCA). We used the *R* language (https://www.r-project.org/) along with the library *stats* to calculate correlation coefficients. The Hierarchical clustering and heatmap were done using the library *ComplexHeatmap*, also written in *R*. In the same manner, PCA was carried out in R by using the library *PCAtools*.

Hub associated genes. Each of the hubs was associated with some reaction (enzyme or transporter) and hence with some gene (or a group of genes). We looked for those genes in the Virtual Metabolic Human website (https://www.vmh.life), which is a database based on information provided by constraint-based stoichiometric models of human metabolism. We manually annotated them to our network, and thus hubs ended up linked to gene IDs.

Pathway enrichment analysis. For the functional analysis of hub genes, we used the R packages ClusterProfiler (Yu *et al.* 2012) and ReactomePA (Yu & He 2016).

High-performance computing software and infrastructure. Distributed computing was implemented by using the Python package *Ray*. All computations were carried out at the National Laboratory for High-Performance Computing (NLHPC) of Chile.

Extracting differential gene expression values from databases. Genes displaying differential abundance in response to glutamatergic neurotransmission were extracted from Supplementary Material reported in (Hasel *et al.* 2017), using the following threshold reported for the astrocyte: fold-change (stimulated/basal) ≥1.3 or ≤0.77 and p-adjusted-SSS-value < 0.05. Differentially abundant genes reported with or without TBOA treatment were merged into a single gene set. For the neuron, the same parameters were used for comparable results. The same procedure was used to extract genes showing with differential abundance in response to brain aging in the astrocyte and neuron (Consortium 2020). We used the threshold reported by the authors at: age coefficient threshold at 0.005 reported by authors as equivalent to a 10%-fold change and an FDR cutoff of 0.01. Given that the abovementioned studies used different RNA-seq approaches (Hasel and collaborators (Hasel *et al.* 2017) performed RNA-Seq of whole cell samples, while the Tabula Muris Consortium (Consortium 2020) used single-cell RNA-Seq), we used the fold-change reported by the authors as significant differential expression and separated each group into up or downregulated after glutamatergic neurotransmission or brain aging, in each cell type.

Mouse ortholog search for hub genes. Hub associated genes; denominated *hub genes* were originally linked to a human entrez gene ID (see above). We used the g:Profiler tool (Kolberg *et al.* 2020; Raudvere *et al.* 2019) at https://biit.cs.ut.ee/gprofiler/gost, and used the g:Orth Orthology search tool to transform human entrez gene IDs into mouse orthologs. This tool delivers the official gene symbol and Ensembl mouse IDs. The resulting mouse ortholog set was cross referenced with the hub genes set, and the intersection resulted in the four *differential hub gene* sets: 1) Differential hub genes after *glutamatergic neurotransmission* in the: a) Neuron, b) Astrocyte; and 2) Differential hub genes regulated during *brain aging* (aged/young) in the: a) Neuron, b) Astrocyte.

KEGG Pathway enrichment analysis. The ClueGO (Bindea *et al.* 2009) plugin in Cytoscape (Shannon *et al.* 2003) was used. Mus musculus [10090] was selected, and for each subset mentioned above (1a, 1b, 2a, 2b), a separate analysis was performed, using two clusters: one

for upregulated genes and the second for downregulated genes. The KEGG database from 13 May 2021 was used, the minimum number of genes per cluster was set as 2, and all other parameters were left as default. Resulting enriched KEGG pathways were manually curated to exclude terms that were unrelated to the nervous systems (see Supplementary Figures 1-4 for uncurated files).

ACKNOWLEDGEMENTS

We thank the National Laboratory for High-Performance Computing (NLHPC) of Chile (ECM-02) for providing supercomputing infrastructure. This work was funded by: FONDAP Geroscience Center for Brain Health and Metabolism (15150012 to CGB); ANID FONDECYT Postdoctoral 3180180 (to DLL) and 3200726 (to AA); ANID FONDECYT Regular 1200029 (to LFB); ANID FONDECYT Regular 1211902 and CEDENNA through Financiamiento Basal para Centros Científicos y Tecnológicos de Excelencia (grant AFB180001) (to FT and MK); and Beca Santander Movilidad Internacional Profesores, Quantum Materials for Energy Efficient Neuromorphic Computing (Q-MEEN-C), US Department of Energy, Office of Science, and Basic Energy Sciences under Award #DE-SC0019273 (to FT). We also thank Manuel I. Muñoz-González for programming the distributed high-performance code in Python.

REFERENCES

Ait-El-Mkadem, S., Dayem-Quere, M., Gusic, M. et al. (2017) Mutations in MDH2, Encoding a Krebs Cycle Enzyme, Cause Early-Onset Severe Encephalopathy. *Am J Hum Genet* **100,** 151-159.

Amelio, I., Cutruzzola, F., Antonov, A., Agostini, M. and Melino, G. (2014) Serine and glycine metabolism in cancer. *Trends Biochem Sci* **39,** 191-198.

Attwell, D. and Laughlin, S. B. (2001) An energy budget for signaling in the grey matter of the brain. *Journal of Cerebral Blood Flow & Metabolism* **21,** 1133-1145.

Baeza-Lehnert, F., Saab, A. S., Gutierrez, R. et al. (2018) Non-Canonical Control of Neuronal Energy Status by the Na+ Pump. *CMET***,** 1-18.

Bélanger, M., Allaman, I. and Magistretti, P. J. (2011) Brain energy metabolism: focus on astrocyte-neuron metabolic cooperation. *Cell metabolism* **14,** 724-738.

Benayoun, B. A., Pollina, E. A. and Brunet, A. (2015) Epigenetic regulation of ageing: linking environmental inputs to genomic stability. *Nature Reviews Molecular Cell Biology* **16,** 593-610.

Bindea, G., Mlecnik, B., Hackl, H. et al. (2009) ClueGO: a Cytoscape plug-in to decipher functionally grouped gene ontology and pathway annotation networks. *Bioinformatics* **25,** 1091-1093.

Bittar, P. G., Charnay, Y., Pellerin, L., Bouras, C. and Magistretti, P. J. (1996) Selective distribution of lactate dehydrogenase isoenzymes in neurons and astrocytes of human brain. *J Cereb Blood Flow Metab* **16,** 1079-1089.

Bonvento, G. and Bolaños, J. P. (2021) Astrocyte-neuron metabolic cooperation shapes brain activity. *CMET* **33,** 1546-1564.

Borgatti, S. P., Everett, Martin G. (2006) A Graph-theoretic perspective on centrality. *Social Networks* **28,** 466-484.

Boumezbeur, F., Mason, G. F., de Graaf, R. A., Behar, K. L., Cline, G. W., Shulman, G. I., Rothman, D. L. and Petersen, K. F. (2010) Altered brain mitochondrial metabolism in healthy aging as assessed by in vivo magnetic resonance spectroscopy. *Journal of Cerebral Blood Flow & Metabolism* **30,** 211-221.

Brautigam, C. A., Wynn, R. M., Chuang, J. L., Machius, M., Tomchick, D. R. and Chuang, D. T. (2006) Structural insight into interactions between dihydrolipoamide dehydrogenase (E3) and E3 binding protein of human pyruvate dehydrogenase complex. *Structure* **14,** 611-621.

Consortium, T. M. (2020) A single-cell transcriptomic atlas characterizes ageing tissues in the mouse. *Nature* **583,** 590-595.

Cunnane, S. C., Trushina, E., Morland, C. et al. (2020) Brain energy rescue: an emerging therapeutic concept for neurodegenerative disorders of ageing. *Nature Reviews Drug Discovery***,** 1-25.

D'Aniello, A., Fisher, G., Migliaccio, N., Cammisa, G., D'Aniello, E. and Spinelli, P. (2005) Amino acids and transaminases activity in ventricular CSF and in brain of normal and Alzheimer patients. *Neurosci Lett* **388,** 49-53.

Dias, G. P., Murphy, T., Stangl, D. et al. (2021) Intermittent fasting enhances long-term memory consolidation, adult hippocampal neurogenesis, and expression of longevity gene Klotho. *Mol Psychiatry*.

Erecinska, M. and Silver, I. A. (1994) Ions and energy in mammalian brain. *Prog Neurobiol* **43,** 37-71.

Fang, X., Lloyd, C. J. and Palsson, B. O. (2020) Reconstructing organisms in silico: genome-scale models and their emerging applications. *Nat Rev Microbiol* **18,** 731-743.

Fernández-Moncada, I., Ruminot, I., Robles-Maldonado, D., Alegría, K., Deitmer, J. W. and Barros, L. F. (2018) Neuronal control of astrocytic respiration through a variant of the Crabtree effect. *Proceedings of the National Academy of Sciences*.

Freeman, L. C. (1978) Centrality in social networks conceptual clarification. *Social Networks* **1,** 215-239.

Gensous, N., Franceschi, C., Santoro, A., Milazzo, M., Garagnani, P. and Bacalini, M. G. (2019) The Impact of Caloric Restriction on the Epigenetic Signatures of Aging. *International Journal of Molecular Sciences* **20,** 2022.

Goyary, D. and Sharma, R. (2008) Late onset of dietary restriction reverses age-related decline of malate-aspartate shuttle enzymes in the liver and kidney of mice. *Biogerontology* **9,** 11-18.

Harris, J. J., Jolivet, R. and Attwell, D. (2012) Synaptic Energy Use and Supply. *Neuron* **75,** 762-777.

Hasel, P., Dando, O., Jiwaji, Z. et al. (2017) Neurons and neuronal activity control gene expression in astrocytes to regulate their development and metabolism. *Nature Communications* **8,** 1-17.

Hegardt, F. G. (1999) Mitochondrial 3-hydroxy-3-methylglutaryl-CoA synthase: a control enzyme in ketogenesis. *Biochem J* **338 (Pt 3),** 569-582.

Hyder, F., Patel, A. B., Gjedde, A., Rothman, D. L., Behar, K. L. and Shulman, R. G. (2006) Neuronal-glial glucose oxidation and glutamatergic-GABAergic function. *J Cereb Blood Flow Metab* **26,** 865-877.

Jiang, T. and Cadenas, E. (2014) Astrocytic metabolic and inflammatory changes as a function of age. *Aging Cell* **13,** 1059-1067.

Jones, M. J., Goodman, S. J. and Kobor, M. S. (2015) DNA methylation and healthy human aging. *Aging Cell* **14,** 924-932.

Katz, L. (1953) A new status index derived from sociometric analysis. *Psychometrika* **18,** 39-43.

Kolberg, L., Raudvere, U., Kuzmin, I., Vilo, J. and Peterson, H. (2020) gprofiler2 -- an R package for gene list functional enrichment analysis and namespace conversion toolset g:Profiler. *F1000Res* **9**.

Latora, V. and Marchiori, M. (2007) A measure of centrality based on network efficiency. *New Journal of Physics* **9**.

Levine, M., McDevitt, R. A., Meer, M. et al. (2020) A rat epigenetic clock recapitulates phenotypic aging and co-localizes with heterochromatin. *eLife* **9,** 299-219.

Lewis, N. E., Schramm, G., Bordbar, A. et al. (2010) Large-scale in silico modeling of metabolic interactions between cell types in the human brain. *Nature Biotechnology* **28,** 1279-1285.

Long, D. M., Frame, A. K., Reardon, P. N., Cumming, R. C., Hendrix, D. A., Kretzschmar, D. and Giebultowicz, J. M. (2020) Lactate dehydrogenase expression modulates longevity and neurodegeneration in Drosophila melanogaster. *Aging (Albany NY)* **12,** 10041-10058.

Mächler, P., Wyss, M. T., Elsayed, M. et al. (2016) In Vivo Evidence for a Lactate Gradient from Astrocytes to Neurons. *Cell metabolism* **23,** 94-102.

Magistretti, P. J. and Allaman, I. (2015) A Cellular Perspective on Brain Energy Metabolism and Functional Imaging. *Neuron* **86,** 883-901.

Mattison, J. A., Colman, R. J., Beasley, T. M. et al. (2017) Caloric restriction improves health and survival of rhesus monkeys. *Nature Communications* **8,** 1-12.

Mattson, M. P. and Arumugam, T. V. (2018) Hallmarks of Brain Aging: Adaptive and Pathological Modification by Metabolic States. *CMET* **27,** 1176-1199.

McCauley, B. S. and Dang, W. (2014) Histone methylation and aging: lessons learned from model systems. *Biochim Biophys Acta* **1839,** 1454-1462.

Minarik, P., Tomaskova, N., Kollarova, M. and Antalik, M. (2002) Malate dehydrogenases--structure and function. *Gen Physiol Biophys* **21,** 257-265.

Newman, J. C., Covarrubias, A. J., Zhao, M., Yu, X., Gut, P., Ng, C.-P., Huang, Y., Haldar, S. and Verdin, E. (2017) Ketogenic Diet Reduces Midlife Mortality and Improves Memory in Aging Mice. *CMET* **26,** 547-557.e548.

Noronha, A., Modamio, J., Jarosz, Y. et al. (2019) The Virtual Metabolic Human database: integrating human and gut microbiome metabolism with nutrition and disease. *Nucleic Acids Res* **47,** D614-D624.

O'Brien, E. J., Monk, J. M. and Palsson, B. O. (2015) Using Genome-scale Models to Predict Biological Capabilities. *Cell* **161,** 971-987.

Odievre, M. H., Chretien, D., Munnich, A. et al. (2005) A novel mutation in the dihydrolipoamide dehydrogenase E3 subunit gene (DLD) resulting in an atypical form of alpha-ketoglutarate dehydrogenase deficiency. *Hum Mutat* **25,** 323-324.

Page, L., Brin, S., Motwani, R. and Winograd, T. (1999) The PageRank Citation Ranking: Bringing Order to the Web. *Stanford InfoLab*.

Pellerin, L. and Magistretti, P. J. (1994) Glutamate uptake into astrocytes stimulates aerobic glycolysis: a mechanism coupling neuronal activity to glucose utilization. *Proc Natl Acad Sci U S A* **91,** 10625-10629.

Raudvere, U., Kolberg, L., Kuzmin, I., Arak, T., Adler, P., Peterson, H. and Vilo, J. (2019) g:Profiler: a web server for functional enrichment analysis and conversions of gene lists (2019 update). *Nucleic Acids Res* **47,** W191-W198.

Reiner, A. and Levitz, J. (2018) Glutamatergic Signaling in the Central Nervous System: Ionotropic and Metabotropic Receptors in Concert. *Neuron* **98,** 1080-1098.

Richardson, N. E., Konon, E. N., Schuster, H. S. et al. (2021) Lifelong restriction of dietary branched-chain amino acids has sex-specific benefits for frailty and lifespan in mice. *Nat Aging* **1,** 73-86.

Roberts, M. N., Wallace, M. A., Tomilov, A. A. et al. (2017) A Ketogenic Diet Extends Longevity and Healthspan in Adult Mice. *CMET* **26,** 539-546.e535.

Schousboe, A. (2019) Metabolic signaling in the brain and the role of astrocytes in control of glutamate and GABA neurotransmission. *Neurosci Lett* **689,** 11-13.

Sen, P., Shah, P. P., Nativio, R. and Berger, S. L. (2016) Epigenetic Mechanisms of Longevity and Aging. *Cell* **166,** 822-839.

Shannon, P., Markiel, A., Ozier, O., Baliga, N. S., Wang, J. T., Ramage, D., Amin, N., Schwikowski, B. and Ideker, T. (2003) Cytoscape: a software environment for integrated models of biomolecular interaction networks. *Genome Res* **13,** 2498-2504.

Solon-Biet, S. M., Cogger, V. C., Pulpitel, T. et al. (2019) Branched-chain amino acids impact health and lifespan indirectly via amino acid balance and appetite control. *Nature Metabolism***,** 1-17.

Stephenson, K. and Zelen, M. (1989) Rethinking centrality: Methods and examples. *Social Networks* **11,** 1-37.

Thiele, I. and Palsson, B. O. (2010) A protocol for generating a high-quality genome-scale metabolic reconstruction. *Nat Protoc* **5,** 93-121.

Voet, D. and Voet, J. G. (2004) *Biochemistry*. John Wiley & Sons, Inc. , United States of America.

Wang, T., Ma, J., Hogan, A. N. et al. (2020) Quantitative Translation of Dog-to-Human Aging by Conserved Remodeling of the DNA Methylome. *Cell Systems***,** 1-17.

Wei, M., Brandhorst, S., Shelehchi, M. et al. (2017) Fasting-mimicking diet and markers/risk factors for aging, diabetes, cancer, and cardiovascular disease. *Sci Transl Med* **9**.

Yu, D., Richardson, N. E., Green, C. L. et al. (2021) The adverse metabolic effects of branched-chain amino acids are mediated by isoleucine and valine. *CMET* **33,** 905-922.e906.

Yu, G. and He, Q. Y. (2016) ReactomePA: an R/Bioconductor package for reactome pathway analysis and visualization. *Mol Biosyst* **12,** 477-479.

Yu, G., Wang, L.-G., Han, Y. and He, Q.-Y. (2012) clusterProfiler: an R Package for Comparing Biological Themes Among Gene Clusters. *OMICS: A Journal of Integrative Biology* **16,** 284-287.

Zampieri, M., Ciccarone, F., Calabrese, R., Franceschi, C., Bürkle, A. and Caiafa, P. (2015) Reconfiguration of DNA methylation in aging. *Mechanisms of Ageing and Development* **151,** 60-70.

Zuend, M., Saab, A. S., Wyss, M. T. et al. (2020) Arousal-induced cortical activity triggers lactate release from astrocytes. *Nature Metabolism***,** 1-26.

Zweig, K. A. (2016) Network Representations of Complex Systems. In: *Network Analysis Literacy: A Practical Approach to the Analysis of Networks,* pp. 109-148. Springer Vienna, Vienna.

FIGURE LEGENDS

Figure 1. Flux optimization determines functional hubs in the neuron-astrocyte metabolic unit (NAMU). a: Reactions considered in the FBA objective function that belongs to the Astrocyte-Neuron Lactate Shuttle (ANLS); astrocyte (left) and neuron (right). **b:** Reactions in the objective that correspond to the Glutamate-Glutamine Cycle (GGC); neuron (left) and astrocyte (right). **c:** sodium efflux considered in the objective. **d-g:** Phenotypic phase planes (PhPPs). The FBA optimal solution is shown as a red-filled circle, and PhPPs are shown as 2-D colored contour levels. All fluxes correspond to micromolar per second. Abbreviations for reaction names are the same as in the original brain model (Lewis et al., 2010). The specific level where the solution resides is shown as a white piece-wise line. NaEx: Neuronal sodium exchange. Lact: Lactate flux from astrocyte to neuron. GluVe: vesicle-released glutamate from the neuron. Obj: objective function. **h:** Bipartite-network representation of the NAMU. Reactions are colored according to their cell, while white nodes denote metabolites. **i:** Flux distribution in each cell (left) and flux allocation (flux-weighted nodes) throughout the network (right). Fluxes were transformed to their absolute values, normalized, and *min-max* scaled to facilitate their comparison and visualization. **j:** same as subplot **i** but considering FBA sensitivities. **k:** Distribution of Absolute Optimality (AO) in the neuron (top) and astrocyte (bottom). The red dashed line by the 90% percentile indicates the cutoff over which we determined optimal hubs. **l:** Non-zero fluxes and non-zero sensitivities sorted (descending) and separated by cell. Enrichment analysis of the genes associated with optimal hubs was done using Reactome Pathway Analysis (**m**) and KEGG (**n**).

Figure 2. Centrality-based nodal contribution to cellular energy metabolism. a: Distribution, by cell, of the nodal centrality contribution to optimal nodes. **b:** Unsupervised hierarchical clustering of the pairwise correlations between nodal contributions. Cells (types of nodes) are annotated on the left-hand side of the heatmap. The Absolute Centrality per node (AC) is shown on the right-hand side of the heatmap. **c**: Dimensionality reduction of the correlation matrix via Principal Component Analysis (PCA). **d:** Distribution of AC in the neuron (top) and astrocyte (bottom). The red dashed line by the 90% percentile indicates the cutoff over which we determine optimal hubs. **e:** Non-zero AC sorted (descending) and separated by cell. Enrichment analysis of the genes associated with central hubs was done using Reactome Pathway Analysis (**f**) and KEGG (**g**).

Figure 3. KEGG pathway enrichment of differential hub genes reveals that the aged neuron displays energetic deficit, dysfunctional neurotransmission, decreased branched-chain amino acid degradation and utilization of ketone bodies, and decreased one-carbon pool levels. KEGG pathway enrichment of differential hub genes was followed by manual curation of associated genes. The results are shown for neurotransmission (top panel) and aging (bottom panel). 1) Oxidative phosphorylation (OxPhos, blue): high OxPhos levels during neurotransmission but low OxPhos levels during aging (blue). 2) Synaptic transmission: upregulated Na/K-ATPase pumps (orange) and glutamate synthesis (green) suggest active repolarization of the neuronal membrane and high glutamate levels. The opposite was observed during aging (lower panel, orange, and green). 3) Ketone body metabolism (yellow): decreased synthesis and increased degradation/utilization during neurotransmission, while observed during aging. 4) Branched-chain amino acid (BCAA) degradation (purple): while differential hub genes involved in the degradation of BCAA were found downregulated during both neurotransmission and aging, *dld*, which encodes for a subunit of BCAA-decarboxylase, an early step in the degradation of all three BCAA was only downregulated during brain aging. 5) One carbon pool (pink): differential hub gene expression associated with one-carbon metabolism suggests high levels of one-carbon pool intermediates during neurotransmission but low during aging.

Figure 4. KEGG pathway enrichment analysis of astrocyte differential hub genes suggests a metabolic switch from aerobic glycolysis to oxidative phosphorylation during aging. 1) Metabolic switch (blue): upregulation of *ldha* during neurotransmission but *ldhb* during aging. *Ldha/b* genes encode for subunits of lactate dehydrogenase, which catalyzes the interconversion of pyruvate into lactate. *Ldha* subunits favor lactate levels and were upregulated during neurotransmission, while *ldhb* favors pyruvate and is upregulated during aging. Also, the major glucose uptake transporter in the blood-brain barrier, encoded by *slc2a1*, was upregulated during neurotransmission only. Instead, during aging, *mdh1/2* encode for enzymes of the malate-aspartate shuttle, which allows transport of NADH into the mitochondrial matrix to provide electrons for the ETC. Both genes were upregulated during aging, in agreement with a high OxPhos rate. 2) Branched-chain amino acid (BCAA) degradation (purple): during neurotransmission, upregulation of slc7a5 was observed (involved in leucine degradation), while during aging, three enzymes involved in BCAA degradation, including *dld*, were downregulated. 3) Ketone body degradation/utilization (yellow): the enzyme encoded by bdh1 catalyzes the interconversion of acetoacetate and β-hydroxybutyrate, the two main ketone bodies, and was upregulated during aging only. 4) Synaptic transmission (green): *abat* encodes for an enzyme

that breaks down GABA into glutamate and is downregulated during aging in the astrocyte. 5) One carbon pool (pink): differential hub gene expression associated with one-carbon metabolism suggests an increase in one-carbon pool during astrocyte aging.

Figure 1

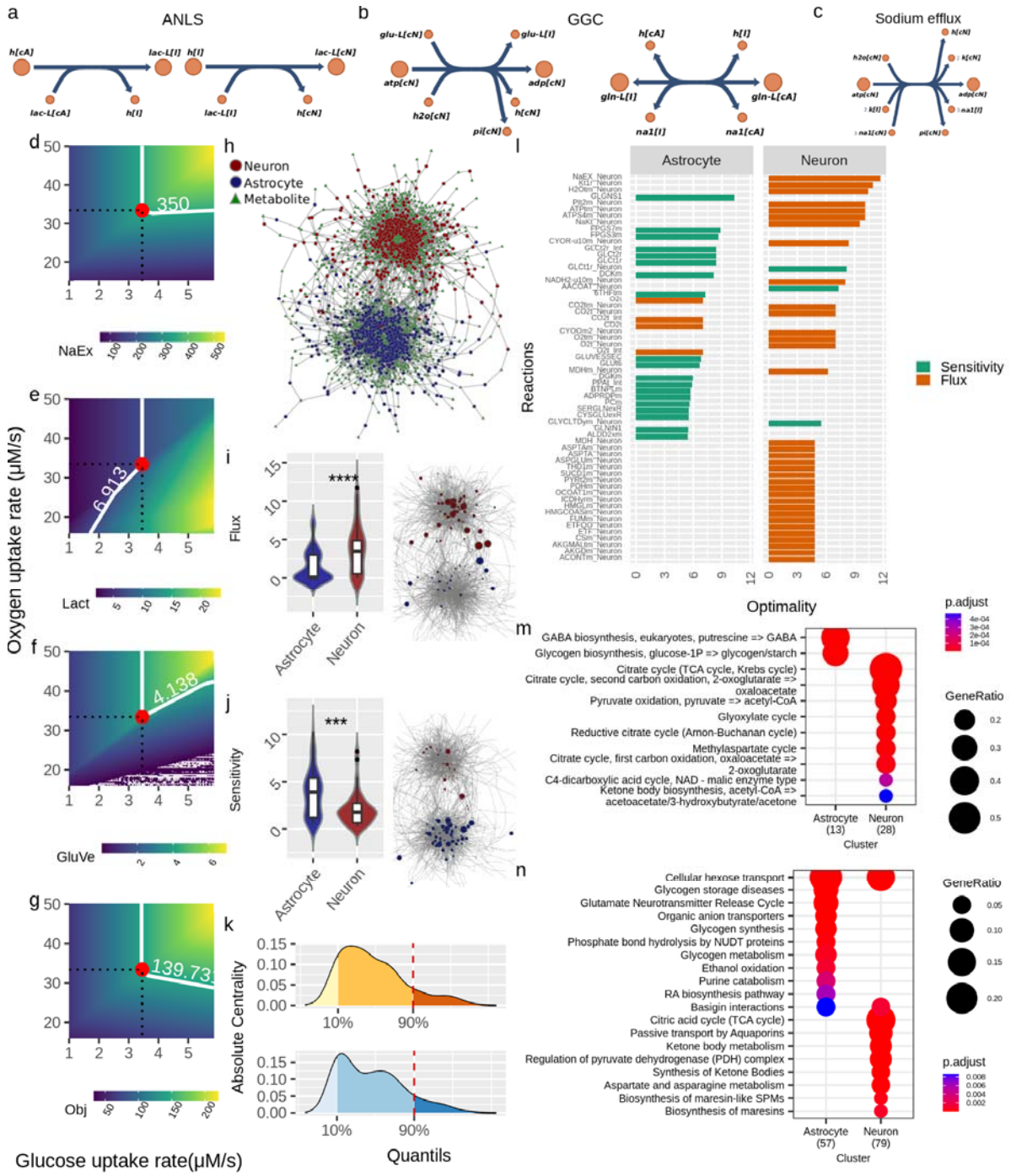
a
ANLS
b
GGC
c
Sodium efflux
d
e
f
g
h
Neuron
Astrocyte
Metabolite
i
j
k
l
Astrocyte
Neuron
Reactions
Optimality
Sensitivity
Flux
m
GABA biosynthesis, eukaryotes, putrescine => GABA
Glycogen biosynthesis, glucose-1P => glycogen/starch
Citrate cycle (TCA cycle, Krebs cycle)
Citrate cycle, second carbon oxidation, 2-oxoglutarate => oxaloacetate
Pyruvate oxidation, pyruvate => acetyl-CoA
Glyoxylate cycle
Reductive citrate cycle (Arnon-Buchanan cycle)
Methylaspartate cycle
Citrate cycle, first carbon oxidation, oxaloacetate => 2-oxoglutarate
C4-dicarboxylic acid cycle, NAD - malic enzyme type
Ketone body biosynthesis, acetyl-CoA => acetoacetate/3-hydroxybutyrate/acetone
Astrocyte (13)
Neuron (28)
Cluster
p.adjust
GeneRatio
n
Cellular hexose transport
Glycogen storage diseases
Glutamate Neurotransmitter Release Cycle
Organic anion transporters
Glycogen synthesis
Phosphate bond hydrolysis by NUDT proteins
Glycogen metabolism
Ethanol oxidation
Purine catabolism
RA biosynthesis pathway
Basigin interactions
Citric acid cycle (TCA cycle)
Passive transport by Aquaporins
Ketone body metabolism
Regulation of pyruvate dehydrogenase (PDH) complex
Synthesis of Ketone Bodies
Aspartate and asparagine metabolism
Biosynthesis of maresin-like SPMs
Biosynthesis of maresins
Astrocyte (57)
Neuron (79)
Cluster
Oxygen uptake rate (μM/s)
Glucose uptake rate(μM/s)
NaEx
Lact
GluVe
Obj
Absolute Centrality
Quantils
10%
90%

Figure 2

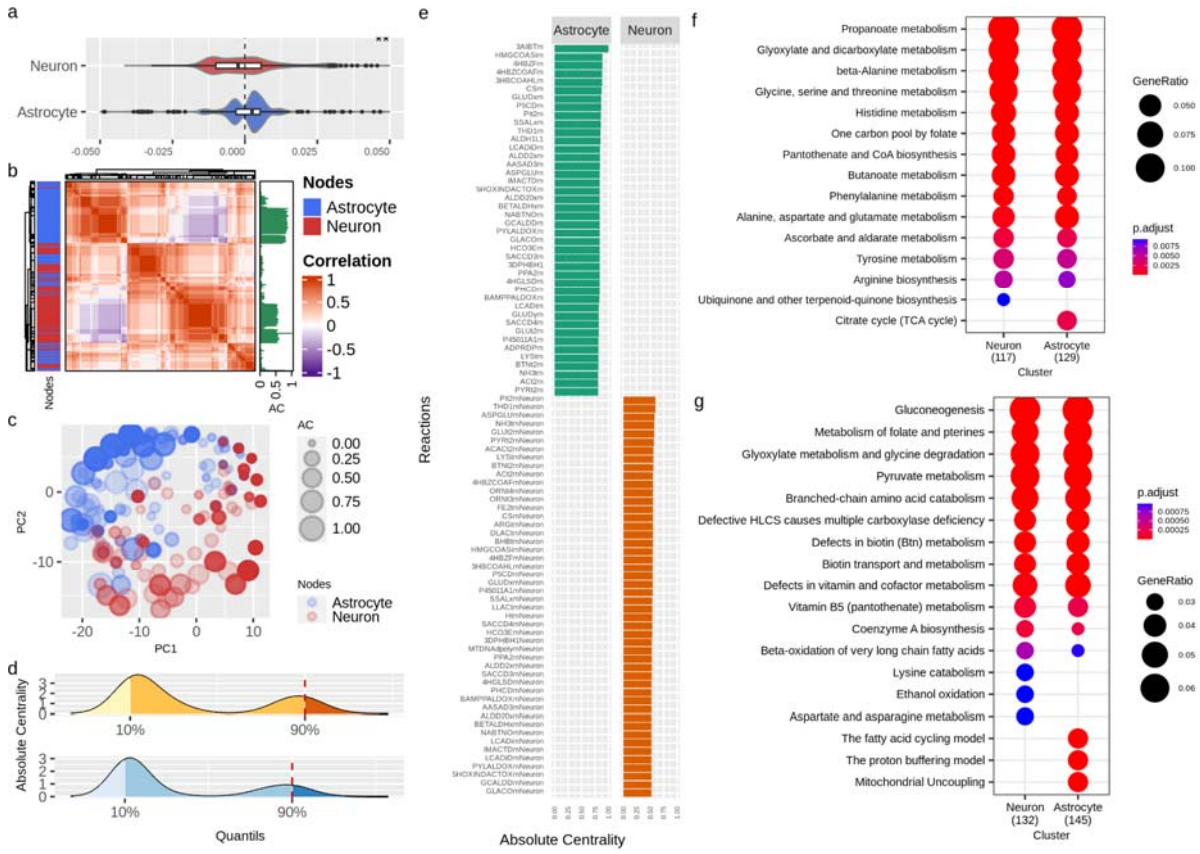
a
Neuron
Astrocyte
-0.050
-0.025
0.000
0.025
0.050
b
Nodes
Astrocyte
Neuron
Correlation
1
0.5
0
-0.5
-1
Nodes
AC
c
PC2
PC1
AC
0.00
0.25
0.50
0.75
1.00
Nodes
Astrocyte
Neuron
d
Absolute Centrality
10%
90%
Quantils
e
Astrocyte
Neuron
Reactions
Absolute Centrality
f
Propanoate metabolism
Glyoxylate and dicarboxylate metabolism
beta-Alanine metabolism
Glycine, serine and threonine metabolism
Histidine metabolism
One carbon pool by folate
Pantothenate and CoA biosynthesis
Butanoate metabolism
Phenylalanine metabolism
Alanine, aspartate and glutamate metabolism
Ascorbate and aldarate metabolism
Tyrosine metabolism
Arginine biosynthesis
Ubiquinone and other terpenoid-quinone biosynthesis
Citrate cycle (TCA cycle)
Neuron (117)
Astrocyte (129)
Cluster
GeneRatio
0.050
0.075
0.100
p.adjust
0.0075
0.0050
0.0025
g
Gluconeogenesis
Metabolism of folate and pterines
Glyoxylate metabolism and glycine degradation
Pyruvate metabolism
Branched-chain amino acid catabolism
Defective HLCS causes multiple carboxylase deficiency
Defects in biotin (Btn) metabolism
Biotin transport and metabolism
Defects in vitamin and cofactor metabolism
Vitamin B5 (pantothenate) metabolism
Coenzyme A biosynthesis
Beta-oxidation of very long chain fatty acids
Lysine catabolism
Ethanol oxidation
Aspartate and asparagine metabolism
The fatty acid cycling model
The proton buffering model
Mitochondrial Uncoupling
Neuron (132)
Astrocyte (145)
Cluster
p.adjust
0.00075
0.00050
0.00025
GeneRatio
0.03
0.04
0.05
0.06

Figure 3

a. Neuron differential hub genes - Neurotransmission

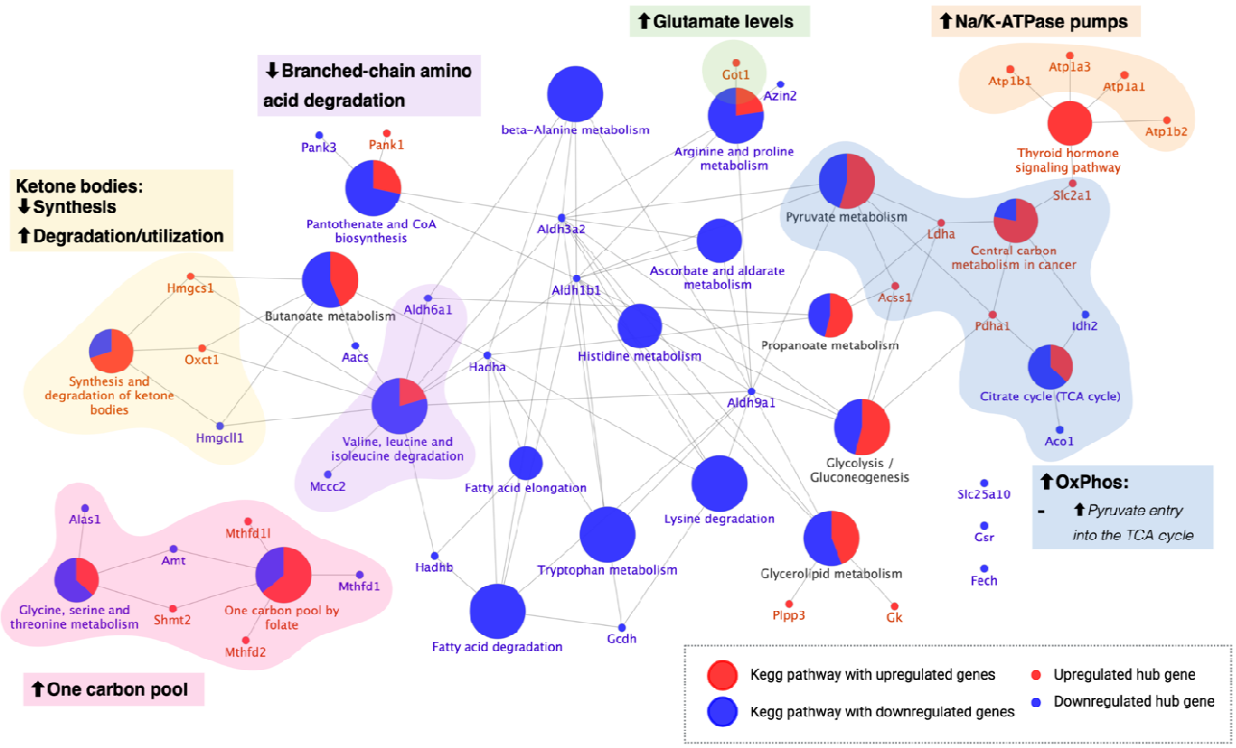

b. Neuron differential hub genes - Aging

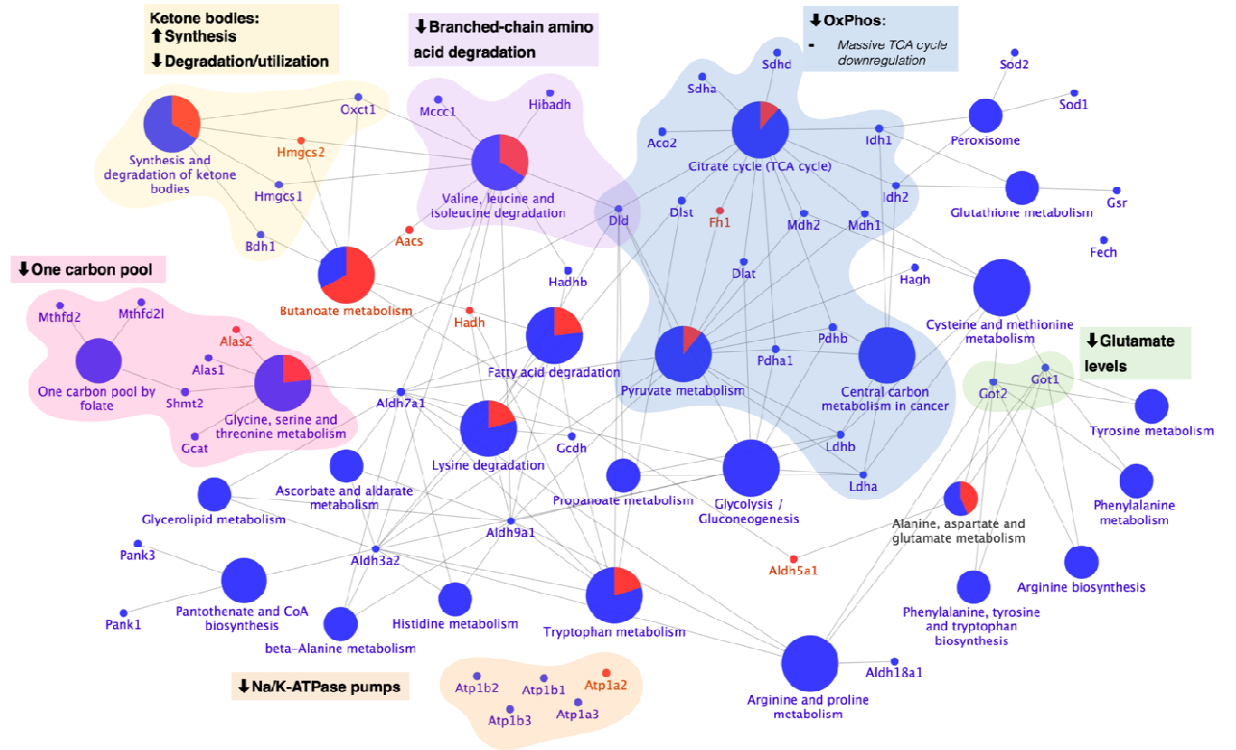

Figure 4

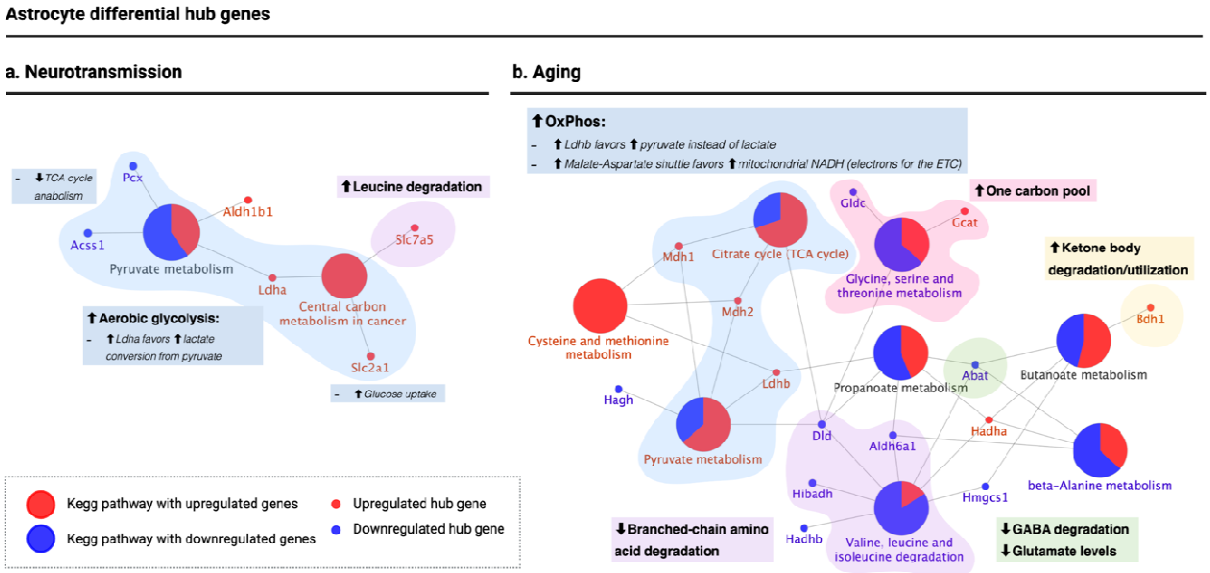
Astrocyte differential hub genes
a. Neurotransmission
- ⬇TCA cycle anabolism
Pcx
Aldh1b1
Acss1
Pyruvate metabolism
Ldha
Central carbon metabolism in cancer
Slc7a5
Slc2a1
⬆Leucine degradation
⬆Aerobic glycolysis:
- ⬆Ldha favors ⬆lactate conversion from pyruvate
- ⬆Glucose uptake
Kegg pathway with upregulated genes
Kegg pathway with downregulated genes
Upregulated hub gene
Downregulated hub gene
b. Aging
⬆OxPhos:
- ⬆Ldhb favors ⬆pyruvate instead of lactate
- ⬆Malate-Aspartate shuttle favors ⬆mitochondrial NADH (electrons for the ETC)
Mdh1
Citrate cycle (TCA cycle)
Mdh2
Cysteine and methionine metabolism
Hagh
Ldhb
Pyruvate metabolism
Gldc
Gcat
Glycine, serine and threonine metabolism
⬆One carbon pool
⬆Ketone body degradation/utilization
Bdh1
Abat
Propanoate metabolism
Butanoate metabolism
Dld
Aldh6a1
Hadha
beta-Alanine metabolism
Hibadh
Hmgcs1
Hachb
Valine, leucine and isoleucine degradation
⬇Branched-chain amino acid degradation
⬇GABA degradation
⬇Glutamate levels